

Available online at [www.sciencedirect.com](http://www.sciencedirect.com)**ScienceDirect**

Procedia Engineering 67 (2013) 261 – 269

**Procedia  
Engineering**[www.elsevier.com/locate/procedia](http://www.elsevier.com/locate/procedia)

7th Asian-Pacific Conference on Aerospace Technology and Science, 7th APCATS 2013

# Numerical Study of Thermochemical Nonequilibrium Flow around Reentry Capsule and Estimation of Aerodynamic Heating

Y. Matsuda<sup>a,\*</sup>, H. Kihara<sup>b</sup>, K. Abe<sup>b</sup><sup>a</sup>Graduate School, Department of Aeronautics and Astronautics, Kyushu University, Fukuoka 8190395, Japan ;<sup>b</sup>Department of Aeronautics and Astronautics, Kyushu University, Fukuoka 8190395, Japan

## Abstract

Numerical simulation of the flow fields was performed for the mission of Apollo AS-202 to investigate the influence of the laminar-turbulent transition position in the boundary layer around a reentry capsule on the heat flux at the wall. For this purpose, we intentionally varied the laminar-turbulent transition position and the obtained results were compared. According to the simulation result, in the turbulent case, heat flux value is about 1.4 times at maximum compared with the laminar case. It turned out that the transition position had a large influence on the heat flux at the wall, particularly in the forebody region. On the other hand, in the afterbody region, some discrepancies were seen compared with the flight data.

© 2013 The Authors. Published by Elsevier Ltd. Open access under [CC BY-NC-ND license](https://creativecommons.org/licenses/by-nc-nd/4.0/).

Selection and peer-review under responsibility of the National Chiao Tung University

**Keywords:** Reentry; Aerodynamic Heating; Thermochemical nonequilibrium; Chemical Reaction; Baldwin-Lomax model

## Nomenclature

$V$	velocity (m/s)
$M$	Mach number
$t$	time history (s)
$T$	temperature(K)
$x, y$	Cartesian coordinate in longitudinal and lateral directions
$y^+$	nondimensional distance from wall surface, $u_\tau \rho y / \mu$
$s$	distance from the stagnation point (m)
<i>Greek symbols</i>	
$\rho$	density(kg/m <sup>3</sup> )

\* Corresponding author. Tel.: +81-92-802-3024; fax: +81-92-802-3024.

E-mail address: [m-yoshiyuki@aero.kyushu-u.ac.jp](mailto:m-yoshiyuki@aero.kyushu-u.ac.jp)

$\mu$	viscosity(N/m <sup>2</sup> ·s)
$\omega$	vorticity(/s)
<i>Subscripts</i>	
$\infty$	freestream condition
$w$	wall
$t$	turbulent

## 1. Introduction

When a capsule reenters an atmospheric environment, a strong shock wave is formed in front of it. Behind the shock wave, a shock layer with very high temperature appears, where a high enthalpy fluid flows around a capsule, resulting in a severe heating environment. Moreover, in an environment where the capsule velocity exceeds 8 km/s such as a super-orbit reentry, there appear complicated phenomena accompanied by the radiation and/or the influence of turbulence.

In such high speed and high altitude flight condition, the gas temperature around capsule reaches the order of 10000 K. Such a high temperature gas is likely to cause an extremely severe heat transfer to the capsule body, which is called aerodynamic heating. Aerodynamic heating is mainly brought by the convection and the radiation under high temperature gas condition. Concerning the convective heat transfer, the effect of turbulence is one of the most important problems. When the atmospheric entry speed exceeds 8 km/s, the transition from laminar to turbulence in the boundary layer may occur, resulting in a large increasing of aerodynamic heating. However, there still remain several issues to be further investigated. For instance, in the case of the Apollo reentry capsule, the amount of mass loss of the ablator had reached the about twice of the prediction.

Based on this background, the present study focuses especially on further development of the prediction strategy of the aerodynamic heating. In this study, we introduce the Baldwin-Lomax model<sup>[1]</sup> to account for the effect of turbulence. The computational results for four turbulent transition cases are compared with the flight data of Apollo AS-202 (see Fig.1), and we discuss the validity of the present numerical model.

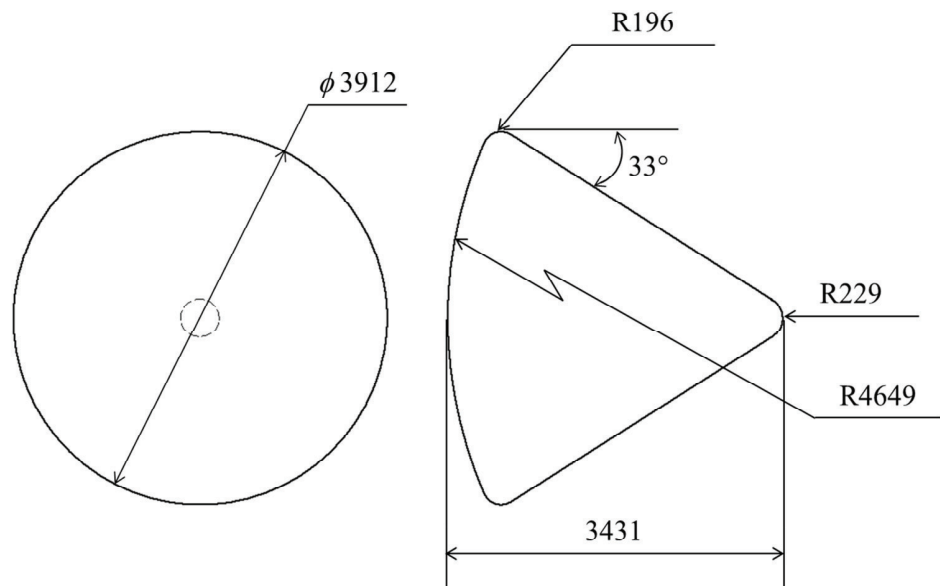


Figure1: Schematic drawing of the outer mold line of capsule as modeled in this study. All dimensions in mm

## 2. Flow Characteristics and Modeling

In this study, we verified the influence of laminar-turbulent transition position of the boundary layer on the flow around a reentry capsule. Note that the laminar-turbulent transition position was assumed in advance in the present calculations for simplicity.

### 2.1. Flow-field model

We assumed that the flow was continuum and it could be described with the compressive Navier-Stokes equation. We used the SLAU method for evaluating the convection term, and we used both the Shock Fix method and the Entropy Fix method in order to avoid any numerical instability and unphysical solution. Moreover, we increased the numerical accuracy by using MUSCL interpolation. Besides, the flow was assumed to be axisymmetric and then the angle of attack assumed was set to 0 degree on the basis of the cone part vertex of Apollo AS-202 that was our analysis object.

We adopted the four-temperature model where temperature was divided into translational, rotational, vibrational, and electron temperatures. Note that the electronic excitation temperature was assumed to be equal to the electron temperature. In the present calculations, the characteristic time of a flow is thought to be comparable to those of the chemical reactions. Therefore, the flow field is supposed to be in thermochemical nonequilibrium.

### 2.2. Turbulence model

In this study, since we aim to investigate how turbulence influences the heating rate at the body surface, we used the Baldwin-Lomax model<sup>[1]</sup> that is one of the simplest models.

### 2.3. Laminar-turbulence transition position

We investigated the following four kinds of the laminar-turbulent transition positions.

Case 1) Laminar flow: This case assumed that the boundary layer is fully laminar. It means that the flow does not transit from laminar to turbulence for the whole region.

Case 2)  $s=2.0[\text{m}]$  ( $s$  is a distance from the stagnation point): This case assumed that the boundary layer transits from laminar to turbulence at the point of  $s=2.0[\text{m}]$ .

Case 3)  $s=3.0[\text{m}]$ : This case assumed that the boundary layer transits from laminar to turbulence at the point of  $s=3.0[\text{m}]$ .

Case 4) Turbulent flow: This case assumed that the flow is fully turbulent for the whole region. (The boundary layer transits from laminar to turbulence at the point of  $s=0[\text{mm}]$ .)

Note that Case 2 and Case 3 were selected so that the transition point might come before and behind the position of the shoulder of the body, respectively.

## 3. Result and Discussion

### 3.1. Calculation condition

The initial conditions were set up based on the flight data<sup>[2,3]</sup>. Those are the points where heat flux at the wall was reported to be large during the reentry trajectory of Apollo AS-202 command module. The time histories of the altitude and the speed of Apollo AS-202 are shown in Figure 2 and the free-stream conditions are shown in Table 1. Note that the time of the launch of Apollo AS-202 is set to  $t=0[\text{s}]$ , and the time from that is set to time history  $t[\text{s}]$ .

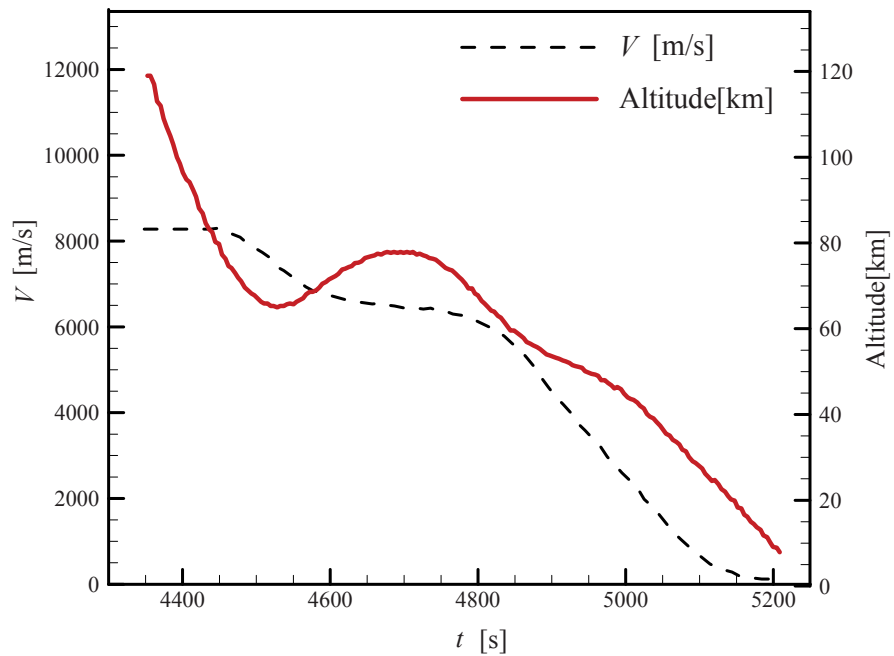


Figure 2: Time history of Altitude and velocity from launch

Table 1: AS-202 trajectory points and free-stream conditions

$t$ [s]	Altitude[km]	$V$ [km/s]	$M$	$\rho_{\infty}$ [kg/m <sup>3</sup> ]	$T_{\infty}$ [K]
4500	70.0	7.92	26.2	$1.52 \times 10^{-4}$	227
4700	77.2	6.49	22.7	$2.45 \times 10^{-5}$	203
4875	54.6	5.07	15.6	$6.16 \times 10^{-4}$	262

### 3.2. Grid system

The presently-used grid system is shown in Figure 3. It covered the whole region surrounding the Apollo AS-202 capsule, though the wake-flow region behind the rear apex of the body was not included in this study. The number of the grid nodes was  $197 \times 209$ . In order to resolve the turbulent boundary layer properly, the first grid point next to the wall surface was located at  $y^+ < 1$ .

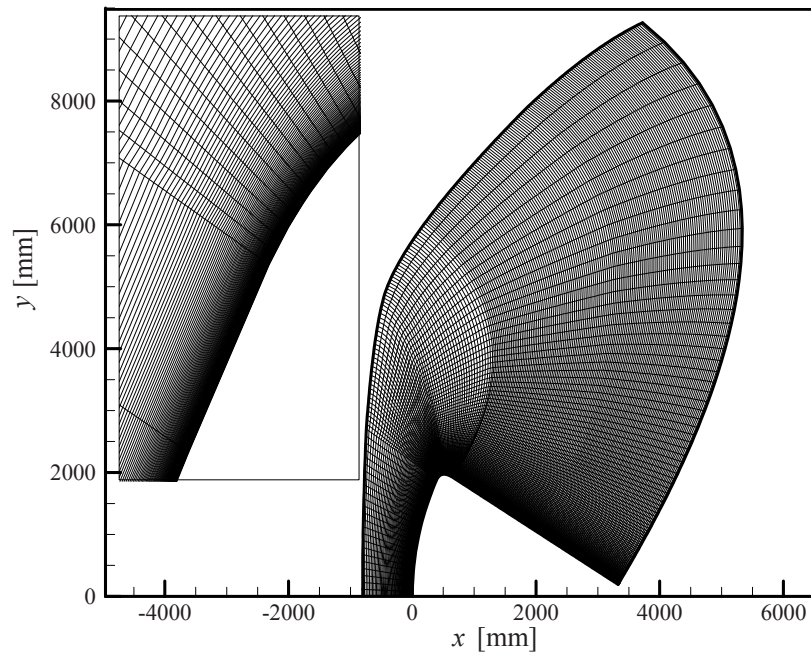


Figure 3: Grid for flow-field calculation

### 3.3. Grid system

The calculation region is surrounded by the following four boundaries:

- The body surface is no-slip, isothermal and non-catalytic wall. The flow velocity is set to 0 [m/s] and the wall temperature is set to 800 [K].
- At the inflow boundary, velocity, density, temperature, and chemical constitution are specified based on the free-stream conditions and the flight data at each altitude shown in Table 1.
- At the outflow boundary, we determine the flow properties in the supersonic region using the 0th extrapolation. On the other hand, although it is not always thought to be reasonable to adopt the same manner in the subsonic region, we employ an easy way to use the values that were increased 0.5 times in this study.
- Axisymmetric condition is used for the center axis.

### 3.4. Computational result

In this section, among three conditions shown in Table 1, the results at  $t = 4500$  [s] are picked up as an example. The distributions of the heat flux at the wall surface are compared in Figure 4. From the results, it is readily understood that the heat flux for Case 1, where the flow is assumed to be fully turbulent, is larger than that for Case 4, where the flow is assumed to be fully laminar. However, the change of the transition point does not influence the heat-flux distribution so much.

In order to investigate this issue in detail, the viscosity distributions behind the shock wave in Case 4 are shown in Figure 5. It is found that the eddy viscosity is much smaller than the molecular viscosity in the region passing through the position of  $x = 500$  [mm] that is near the shoulder. This also means that the influence of turbulence in the boundary layer came out only in the region of the forebody under the present computational conditions, and thus no remarkable difference was seen between Case 2 and Case 3.

Moreover, from the comparison of the present results with the flight data on both the windward and lee sides, it turned out that there can be seen some difference between them. Since the actual capsule reentries with some angle of attack, vortices tend to be generated in the afterbody region, resulting in the more active heat exchange. In addition, from the analysis of the MUSES-C capsule, it has been reported that the heat flux by the radiation becomes dominant rather than that by the convection<sup>[4]</sup> in the afterbody region. Therefore, it is considered as a cause that we did not take the effect of the radiation heating into consideration in this analysis.

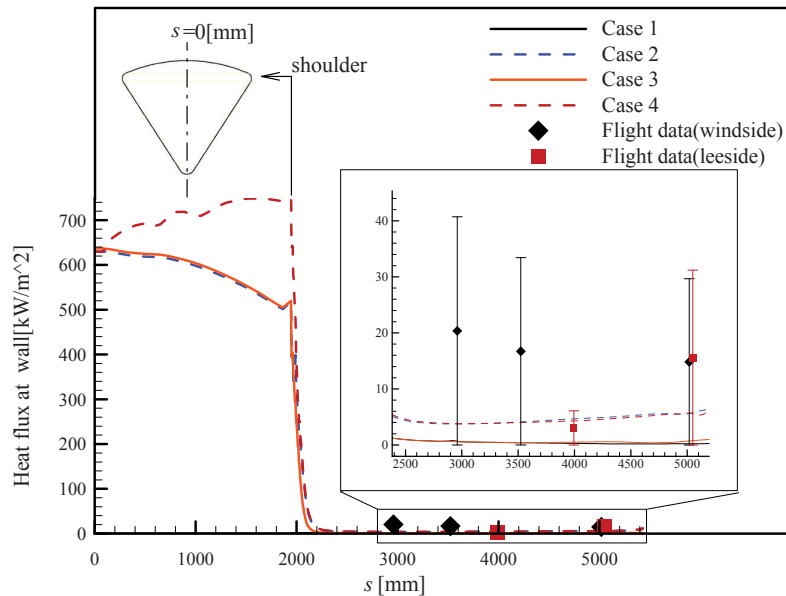


Figure 4: Comparison of the heat flux at the wall at  $t=4500$  [s]

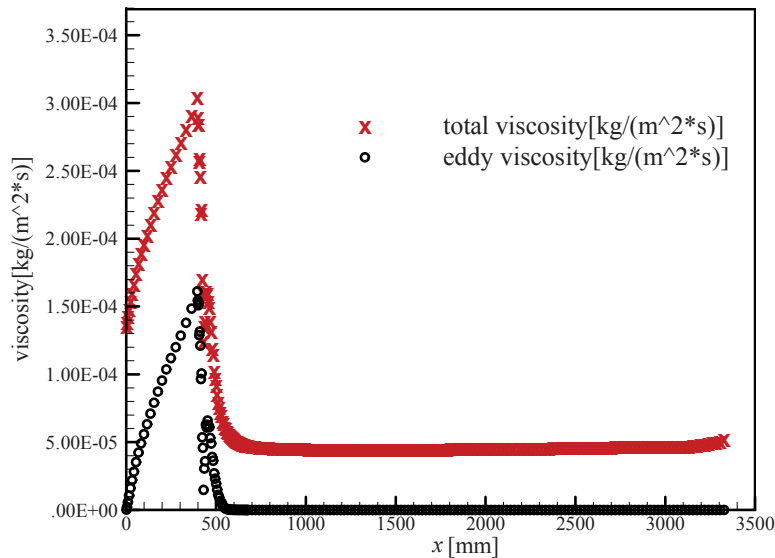


Figure 5: Viscosity distributions behind the shock wave in Case 4

#### 4. Conclusion

We performed the numerical simulation of the flow fields around Apollo AS-202 Command module to investigate the influence of the laminar-turbulent transition position in the boundary layer around a reentry capsule on the heat flux at the wall. For this purpose, we intentionally varied the laminar-turbulent transition position and the obtained results were compared. It turned out that the laminar-turbulent transition has big influence on the heat-flux distribution at the wall, particularly in the forebody region.

Although useful knowledge was obtained from the present study, there still remained several margins to be improved. In fact, some differences were seen between the present results and the flight data. In this study, we assumed the angle of attack to be  $0^\circ$  and thus the flow was assumed to be axisymmetric, though the actual angle of attack was  $18^\circ$  when Apollo AS-202 reentered the earth atmosphere. In addition, the present computational domain did not include the wake-flow region behind the rear apex of the body, resulting in the disappearance of vortices that were expected to be generated there. Another reason might be that we did not take the effect of the radiation heating into consideration in this analysis. These issues are to be improved in future study.

#### Acknowledgements

The computations were mainly carried out using the computer facilities at Research Institute for Information Technology, Kyushu University.

#### References

- [1] Baldwin, B.S., and Lomax, H., "Thin layer approximation and algebraic model for separated turbulent flows," AIAA paper, No.78-257, 1978.
- [2] Michael J. Wright, Dinesh K. Prabhu and Edward R. Martinez, "Analysis of Apollo Command Module Afterbody Heating, Part 1: AS-202" Journal of Thermophysics and Heat Transfer, January-March 2006, pp.16-30.
- [3] Dorothy B. Lee, John J. Bertin and Winston D. Goodrich, "Heat-Transfer Rate and Pressure Measurements Obtained During Apollo Orbital Entries," NASA TN D-6028, October 1970.
- [4] Fujita K., Otsu H., Yamada T. and Abe T., "Assessment of Radiation Reentry Environment around MUSES-C Capsule," Journal of the Japan Society for Aeronautical and Space Sciences, 2003, Volume 51, pp. 419-426

#### Appendix A.

##### A.1. Baldwin-Lomax model

Baldwin-Lomax model is categorized in the group of "eddy viscosity model" and it is often used as an attached boundary-layer turbulence model. In the Navier-Stokes equation used in this study, this model takes transportation by turbulence into consideration by replacing the coefficient of viscosity  $\mu$  with  $\mu + \mu_t$  and the heat conduction coefficient  $K$  with  $K + K_t$ . To use this model, we divide a boundary layer into two layers, an inner layer and an outer layer with reference to the distance  $y$  from the body surface.

## Equations

$$\mu_t = \begin{cases} (\mu_t)_{inner} & y \leq y_c \\ (\mu_t)_{outer} & y \geq y_c \end{cases} \quad (A-1)$$

where  $y_c$  is the position from the surface at which  $(\mu_t)_{inner}$  is equal to  $(\mu_t)_{outer}$

$$(\mu_t)_{inner} \Big|_{y=y_c} = (\mu_t)_{outer} \Big|_{y=y_c} \quad (A-2)$$

The eddy viscosity in the inner region is given by the Prandtl - Van Driest formula:

$$(\mu_t)_{inner} = \rho l^2 |\omega| \quad (A-3)$$

Where

$$l = K_1 y \left[ 1 - \exp\left(-\frac{y^+}{A}\right) \right] \quad (A-4)$$

$$|\omega| = \left| \frac{\partial u}{\partial y} - \frac{\partial v}{\partial x} \right| \quad (A-5)$$

$$y^+ = \frac{y \sqrt{\rho_w \tau_w}}{\mu_w} \quad (A-6)$$

$$\tau_w = \left( \mu \frac{\partial u}{\partial y} \right)_w \quad (A-7)$$

The eddy viscosity in the outer region is given by:

$$(\mu_t)_{outer} = \rho K_2 C_{cp} F_{WAKE} F_{KLEB} \quad (A-8)$$

Where

$$F_{WAKE} = \min \left[ y_{MAX} F_{MAX}, C_{wk} y_{MAX} \frac{u_{DIF}^2}{F_{MAX}} \right] \quad (A-9)$$



Here,  $y_{MAX}$  and  $F_{MAX}$  are determined as follows:

$$F(y) = y|\omega| \left[ 1 - \exp\left(-\frac{y^+}{A}\right) \right] \quad (\text{A-10})$$

$$F(y_{MAX}) = F_{MAX} \quad (\text{A-11})$$

where  $F_{KLEB}$  is the intermittency factor given by

$$F_{KLEB} = \left[ 1 + 5.5 \left( \frac{C_{KLEB}}{y_{MAX}} \right)^6 \right]^{-1} \quad (\text{A-12})$$

On the other hand,  $u_{DIF}$  is the difference between the maximum and the minimum speeds in the velocity profile. Note that for boundary layers, the minimum speed is always set to zero.

$$u_{DIF}^2 = \left( \sqrt{u^2 + v^2}_{\max} - \sqrt{u^2 + v^2}_{\min} \right)^2 \quad (\text{A-13})$$

The model constants used in the above formulas are as follows:

$$\left\{ \begin{array}{l} A = 26 \\ C_{cp} = 1.6 \\ C_{KLEB} = 0.3 \\ C_{wk} = 0.25 \\ K_1 = 0.4 \\ K_2 = 0.0168 \end{array} \right. \quad (\text{A-14})$$